Constant Stress Layer Characteristics in Simulated Stratified Air Flows: Implications for Aeolian Transport

Abstract

Varying thermal atmospheric stability conditions and their effects on shearing flows has long been a subject of interest for researchers working in atmospheric science. The development of new instrument technologies now offers an opportunity to study flows with high spatial and temporal resolutions in wind tunnel atmospheric boundary layers. In the presented study, we use a laser Doppler anemometer within the Trent Environmental Wind Tunnel Laboratory to investigate the influence of thermal stratification on the constant stress layer. Analyses of the thermal stratification represented by the gradient Richardson number and the apparent von Kármán parameter, shear velocity, and the slope of the streamwise velocity profiles reveal strong linear relationships. An exponential relationship between thermal stability and the apparent roughness length is also revealed. Profiles of the streamwise and vertical velocity and turbulence intensity, as well as the dimensionless Reynolds stress, are influenced by the gradient Richardson number. These findings have implications for producing accurate models of sediment entrainment and transport by wind in non-neutral conditions.

Keywords Gradient Richardson number • Law of the wall • Turbulence profiles • Wind tunnel research • Velocity profiles

1. Introduction

Atmospheric stability is altered by the vertical movement of air parcels due to thermal stratification. Unstable thermal atmospheric conditions and accompanying flows are characterized by strong vertical mixing, while convection is suppressed in stable thermal conditions (Frank and Kocurek 1994). In nature, boundary layer flows are heated or cooled by the underlying surface, resulting in non-neutral conditions. The gradient Richardson number (Ri_g) is applied to quantify the atmospheric thermal stability

$$Ri_g = \frac{g}{\theta}\frac{\frac{\partial\theta}{\partial z}}{\left(\frac{\partial u}{\partial z}\right)^2} \qquad (1)$$

where θ is the potential temperature. This parameter can be interpreted as the ratio of buoyancy to shear turbulence. Positive Ri_g values indicate stable conditions, with turbulence attenuated by thermal inversion and compressed eddy size. Negative values refer to unstable conditions, with enhanced turbulence production by thermal convection and elongated eddy size (Garratt 1994, Balsley et al 2007, Li 2010). Several wind tunnel studies have demonstrated that thermal atmospheric stability has a strong influence on the characteristics of the airflow in the near-surface boundary-layer (Ogawa et al. 1981, Marusic et al. 2010, Friedrich et al. 2012, Kim et al. 2020, Sessa et al. 2020, Demarco et al. 2022) and field (Monin and Obukhov 1954, Businger et al. 1971, Frank and Kocureck 1994, Andreas et al. 2006, Högström et al. 2008, Salesky et al. 2013, Li 2018). The Law of the Wall (von Kármán 1931) indicates that under neutral conditions, the velocity profile follows a log-linear law in the constant stress layer as

$$U = \frac{u_*}{\kappa}\ln\left(\frac{z}{z_0}\right) \tag{2}$$

where U is the time-averaged streamwise velocity at an elevation of z, u_* is the shear velocity, and z_0 is the apparent roughness length. However, this law must be corrected for non-neutral conditions (Businger et al. 1971, Frank and Kocureck 1994, Andreas et al. 2006, Högström et al. 2008), to account for the effect of thermal stability on the flow structure (Businger et al. 1971, Wright and Parker 2004). This correction can be carried out by adjusting the von Kármán constant κ. In a neutral atmospheric boundary layer κ is approximately constant, varying within a narrow range between 0.370 and 0.421 (Österlund et al. 2000, Zanoun et al. 2003, McKeon et al. 2004, Morrison et al. 2004, Monty 2005, Nagib et al. 2007, Nickels et a. 2007, Marusic et al. 2010). In non-neutral conditions, however, there is an apparent change in the value of κ, represented as an apparent von Kármán parameter κ_a in the Law of the Wall (Li et al., 2010) as

$$U = \frac{u_*}{\kappa_a}\ln\left(\frac{z}{z_0}\right) \tag{3}$$

or in its differential form as

$$\frac{\partial u}{\partial z} = \frac{u_*}{\kappa_a z} \tag{4}$$

The apparent von Kármán parameter is inversely proportional to a commonly used dimensionless wind shear term $\emptyset_m$ (Monin and Obukhov 1954, Businger et al. 1971), defined as follows

$$\emptyset_m = \frac{\kappa z}{u_*}\frac{\partial U}{\partial z} = \frac{\kappa}{\kappa_a} \tag{5}$$

where $\emptyset_m > 1$ represents stable and $\emptyset_m < 1$ unstable conditions. Based on a field experiment carried out in Kansas, Businger et al. (1971) concluded that $\emptyset_m$ increases slowly with decreasing Ri in unstable conditions ($Ri < 0$). Under stable conditions $\emptyset_m$ increases linearly at a much steeper rate (Businger et al. 1971). From an experiment conducted above seawater, Högström et al. (2008) found that this linear trend can extend into unstable conditions if the magnitude of Ri is very small and $\emptyset_m$ can eventually reach a constant level of about 0.1 under extremely unstable conditions.

Furthermore, the thermal atmospheric stability can affect the apparent roughness length scale and turbulence characteristics. In wind tunnel and field studies the slope of normalized velocity profiles decreases and z_0 increases with increasing thermal stability (Ohya et al. 1996, Ohya 2001, Joffre et al. 2001, Ohya and Uchida 2004). Additionally, the turbulence intensity, shear velocity, and Reynolds stress decrease with increased thermal stability. Herein vertical mixing is reduced due to the damping effect of stable thermal stratification, and these variables are all affected through their interdependency (Joffre et al. 2001, Ohya 2001).

The majority of atmospheric stability experiments have been conducted in the field, assuming steady flow conditions within a certain time period (usually 30 minutes). Attaining these ideal conditions is often challenging due to various mesoscale motions, such as gravity waves, meandering-like motions, and density currents (Mahrt 2007). Such issues can be avoided by conducting experiments in environment-controlled wind tunnels, such as the Environmental Flow Wind tunnel (Enflo) at the University of Surrey (Hancock et al. 2018, Marucci et al. 2018, Sessa et al., 2020), and the thermally stratified wind tunnel (TSWT) at Kyushu University (Ohya et al. 1996, Uchida and Ohya 1999, Hara et al., 2009). These tunnels have an air heating unit at the entrance and temperature control panels on the working section floors to create a thermal stratification. In laboratory experiments it is very difficult, however, to profile the flow characteristics at a very fine spatial (millimetre) scale in a constant stress layer that is only a few centimetres thick. Crosswire probes for example, as used in constant temperature anemometry, are simply too large. Therefore, the available experimental data that describes thermally driven adjustment within the thin constant stress layer that adjoins the bed surface is limited.

Recent aeolian studies indicate that changes in the turbulence intensity can significantly affect the entrainment and transport of sediment around the threshold velocity (Rana et al., 2020; Zheng et al., 2020). One should expect atmospheric stability to play an important role in modelling entrainment threshold conditions, since atmospheric stability moderates the development of turbulence within the constant stress layer where aeolian sediment entrainment occurs. The time-averaged vertical wind speed is typically considered to be zero and thus to have a negligible effect on sediment entrainment in neutral conditions. This assumption is expressed in virtually all sediment transport models, in which streamwise flow parameters such as the time-averaged streamwise velocity and shear velocity, are related to the threshold for motion or sediment transport rate. However, atmospheric instability generates strong horizontal and vertical shear generation of turbulence resulting in a non-zero time-averaged vertical wind velocity near the surface (Coulter and Martin, 1996) Thus, in unstable conditions, vertical velocity may affect the initiation of motion and be attributable to the invalidity of existing formulas for sediment transport. For example, one may infer that an upward velocity increases the lift force thereby reducing the threshold shear stress for entrainment (Yang and AL-Fadhly, 2021).

Moreover, the performance of commonly applied models of sediment transport (Bagnold 1936, Kawamura 1951, Zingg 1953, Owen 1964, Lettau and Lettau 1978, Sørensen 2004, Sherman et al., 2012) and saltation-induced dust emission (Ginoux et al. 2001, Shao 2001, LeGrand et al. 2019) are strongly dependent upon an accurate assessment of the shear velocity and threshold shear velocities. A common practice among most aeolian scientists is to measure the wind profile within the constant stress layer and to adopt the Law of the Wall to derive the shear velocity. As the Law of the Wall requires adjustment in non-neutral conditions to account for the variability of the thermal stratification, the apparent von Kármán parameter needs to be adapted to derive an accurate shear velocity value for aeolian studies. However, previous wind tunnel studies have been conducted at very low wind speeds (typically smaller than 2 m s^{-1}) to generate a wide range of Richardson numbers. In the context of aeolian transport studies, these wind speeds are too low to initiate the motion of sediment particles and thus the results from such studies are not directly applicable to aeolian sediment transport.

This study aims to address this shortcoming by examining the flow characteristics within the constant stress layer in clear air at wind speeds high enough to entrain fine sand particles under thermally unstable, neutral, and stable conditions in an environmental-controlled wind tunnel. We assess how the thermal atmospheric stability, represented by the gradient Richardson number, affects vertical profiles of average velocity, turbulence intensities, dimensionless Reynolds stress profiles within the constant stress layer, as well as the apparent surface roughness and the apparent von Kármán parameter. Finally, we explore the implications of these differences in flow characteristics between thermally unstable and stable conditions on aeolian sediment transport.

2. Methods

2.1 Wind tunnel experiment

The experiments were conducted in the Environmental Wind Tunnel (TEWT) facility at Trent University in Canada. The laboratory is specifically designed to simulate the atmospheric boundary layer (ABL) in clean air and during sediment transport. This suction-type, straight-line wind tunnel is positioned in a climate-controlled room with an adjustable temperature range from -10°C to 30°C and humidity control. During the experiments, the climate-conditioned air in the room was drawn in through a honeycomb air straightener at the entrance of a contraction bell to eliminate ambient turbulence. The intake air was thus contracted and accelerated by a Venturi effect. Before it reached the working section, the air passed over a roughness plate to induce shear and extend the boundary-layer depth.

The working section is 13.5 m long, 0.71 m high and 0.76 m wide. Two 30 mm high metal rails were installed at the inner and outer sides of the test section floor to contain a levelled bed of well-sorted sand with median diameter of 0.55 mm. A 9-blade vane-axial fan installed in the drive section drew the air through the tunnel instead of blowing it, to avoid the propagation of turbulent eddies from the fan blades through the test section. Freestream wind speeds can be controlled up to 20 m s^{-1} by programming the fan speed, however we only ran our experiments between 4 ms^{-1} and 6 ms^{-1}. These velocities translate to shear velocities between 0.15 ms $^{-1}$ and 0.26 ms $^{-1}$, which are sufficient to entrain fine sand particles yet below the fluid threshold shear velocity for the coarse sand used in the tunnel (Kok et al. 2012). The coarse bed texture was selected to prevent particle entrainment at the wind speeds used, and thus, remove the influence of the grain borne stress on the wind speed profile. As the flow was much faster than previous studies, the time given to the airflow to interact with a cooled or warmed bed surface was much shorter, which limited the range of Richardson number. More detailed descriptions of the wind tunnel are provided in previous publications (Nickling and Neuman 1997, McKenna Neuman 2003, Neuman 2004, Li and McKenna Neuman 2012).

We conducted two sets of experiments. The first set (Set 1) examined the stability effect on air flows. All sampling (Fig. 1) was carried out 13 m downwind from the leading edge of the working section, where the boundary-layer was fully developed. Instantaneous horizontal u and vertical w wind velocities were measured using a customized Dantec 2-D laser Doppler anemometer (LDA); c.f. Li and McKenna Neuman (2012) for a detailed description of this instrument. To measure the wind velocity, the air flow was seeded with micron sized, neutrally buoyant particles produced from a fog machine (Atari HZ-350). Velocity data were sampled in a vertical sequence of 9-15 points, starting 4-6 mm above the bed surface (depending on the LDA data rate) and moving vertically in small logarithmic increments up to a height of 22 mm. In total 16% of the boundary-layer thickness δ was profiled, a region of the flow wherein the

Reynolds stress was assumed to be constant. The sampling scheme was designed to reduce the LDA traverse time between measurement positions, as required to capture a velocity profile with a constant temperature gradient; the sampling duration was either 11 or 15 seconds at each elevation to measure the average velocity and its instantaneous fluctuation. The freestream velocity in the streamwise direction u_∞ was measured with a pitot tube at a fixed height of 0.2 m above the surface (c.f. Fig. 1). Temperature profiles were measured using three T-type thermocouples placed 0.05 m downstream of the LDA profile at elevations of 7.5 mm, 19 mm, and 179 mm (c.f. Fig. 1). A thermos-humidity sensor (Vaisala HMP235) and a pressure sensor (Vaisala PTB100B) were installed on the external wall of the wind tunnel to measure the room temperature, relative humidity, and atmospheric pressure.

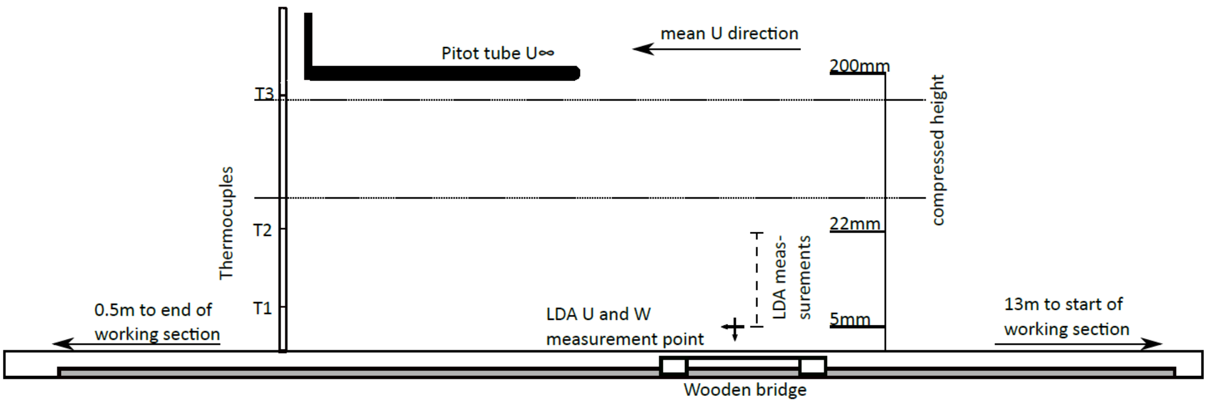

Fig. 1 Schematic of the experimental setup.

To establish unstable conditions, heating mats (Vivosun Seeding Inc.) were placed onto the entire working section floor, onto which the coarse sand bed was placed. Before the start of each experiment, this sand bed was heated to ≈ 40°C and then covered with rigid foam insulation boards (Owens Corning Fiberglas Inc.) to maintain the sand temperature. After that, the room temperature was lowered to ≈ 5°C. The experiments started immediately after the insulation boards were removed. Over the course of seven replicate experiments, sampling continued until the air-sand temperature difference became insignificant, providing a total of 42 wind profiles with varied gradient Richardson number (R) representing a range of unstable ABL conditions.

For stable conditions, to maintain the sand surface temperature as long as possible, the surface was sprayed with a water mist, chilled to ≈ -8°C and then allowed to sit overnight. On the following morning, the frozen surface was covered with insulation boards while the room temperature was heated to ≈ 20°C. Once again, the experiments began immediately after the insulation boards were removed, and seven experiments were carried out with 42 wind profiles sampled.

Experiments in neutral conditions were conducted without any thermal treatment, while a semi-constant room temperature 13°C +/- 1°C was maintained. Before each experiment, the wind tunnel was operated at low velocity to fully mix the air inside the laboratory and create a thermally homogenous environment. Overall, we captured twelve, 9-point wind profile measurements within the constant stress layer.

In the second sets of experiments (Set 2), we sampled 96 additional neutral profiles to (i) achieve a statistically significant value for κ under neutral conditions which can be compared to other wind tunnel studies; (ii) validate the measurements obtained with the thin, near-bed profile; and (iii) precisely define the vertical limit for the constant stress layer. All settings were the same as for the neutral experiments in the first set, with the exception that wind profiles were measured over fifteen elevations ranging from 4 mm to 184 mm with a measurement duration of 15 seconds at each position.

2.2 Variable Derivation

The transition time-weighted streamwise and vertical velocities (U, W), as well as the root-mean-squared turbulent velocity fluctuations and their cross product (u', w', $u'w'$) for each LDA position, were calculated by the Dantec BSA Flow software. The normalized velocities U/U_∞ and W/U_∞ were calculated with U_∞ obtained from the Pitot tube measurements. Consistent with Li and McKenna Neuman (2012) who made similar measurements with the same instrument, turbulence intensity (T_u, T_w) and the dimensionless Reynolds stress term T_{uw} are defined as follows

$$T_u = \frac{u\prime}{U_\infty} \tag{6}$$

$$T_w = \frac{w\prime}{U_\infty} \tag{7}$$

$$T_{uw} = \frac{\sqrt{-\overline{u\prime w\prime}}}{U_\infty} \tag{8}$$

As the Reynolds stress profiles were obtained within the constant stress layer, a spatially-averaged Reynolds stress term $-< \overline{u'w'} >$, can be used to estimate the shear velocity u_* (Nezu et al. 1997):

$$u_* = \sqrt{-<\overline{u'w'}>} \quad (9)$$

In accordance with the Law of the Wall, as described by Eqn. 2, the velocity profile measurements can be used to obtain two least-square regression coefficients, *m* and *n*, by fitting a log-linear function as,

$$U = m\, ln(z) + n \quad (10)$$

Following Bauer et al. (1992), both the apparent von Kármán parameter κ_a and the apparent roughness length z_0 for different stability conditions can be determined using the following two equations, respectively,

$$\kappa_a = \frac{u_*}{m} \quad (11)$$

and

$$z_0 = \exp(-n/m) \quad (12)$$

The velocity gradient ∂u/∂z at location *z* can be derived using

$$\frac{\partial U}{\partial z} = \frac{m}{z} \quad (13)$$

From our observations and those by Ohya (2001), Li (2018), and Cheng et al. (2021), the potential temperature θ profile also follows a log-linear function as

$$\theta = a\, ln(z) + b \quad (14)$$

where *a* and *b* are least-squares regression coefficients. The local potential temperature at any height can also be estimated using the above equation. Like wind gradient estimations, the thermal gradient at location *z* is obtained using

$$\frac{\partial \theta}{\partial \mathrm{z}} = \frac{a}{z} \quad (15)$$

From the thermal and velocity gradients, the gradient Richardson number at *z* can be estimated using Eq. 1.

As Ri_g is a function of *z*, an integrated gradient Richardson number *Ri* is proposed to evaluate the overall effect of atmospheric stability, based on the gradient Richardson numbers from z_0 to an upper limit of constant stress layer, 0.022 m (i.e., ~ 0.16δ),

$$Ri = \frac{1}{0.022 - z_0} \int_{z_0}^{0.022} Ri_g \, dz \quad (16)$$

3. Results

3.1 Influence of atmospheric stability on vertical profiles of flow velocity, turbulence intensity and Reynolds stress.

Altogether 96 normalized streamwise (U/U_∞) and vertical (W/U_∞) velocity profiles were collected in the first set of experiments to explore the full range of stability conditions. We found that all vertical U/U_∞ profiles within the constant stress layer were log-linear, as described by Eq. 10, with each log-linear regression having an R^2 value above 0.9. Due to difficulty in displaying all 96 profiles, we derived bin-averaged U/U_∞ and W/U_∞ profiles in stable, neutral, and unstable conditions, respectively, and plotted them in Figs. 2a and 2b. As shown in Fig. 2 (a), the normalized streamwise velocity at any given elevation decreases with increasing *Ri*. In moving away from the bed surface, however, the effect of atmospheric stability gradually diminishes so that at 0.16δ the normalized streamwise velocities approach convergence. On average, the standard deviation of U/U_∞ lies between 1% and 2%, though under unstable conditions it is generally smaller than for stable conditions. Fig. 2 (b) shows that W/U_∞ remains almost constant around 0 under neutral conditions, independent of elevation. As expected, the normalized vertical velocity increases under unstable conditions ($Ri < 0$) from near 0 adjacent to the bed surface to 0.0043 at 0.16δ, and is negative for stable conditions ($Ri > 0$), decreasing in absolute magnitude with increasing elevation from -0.0057 to -0.0024.

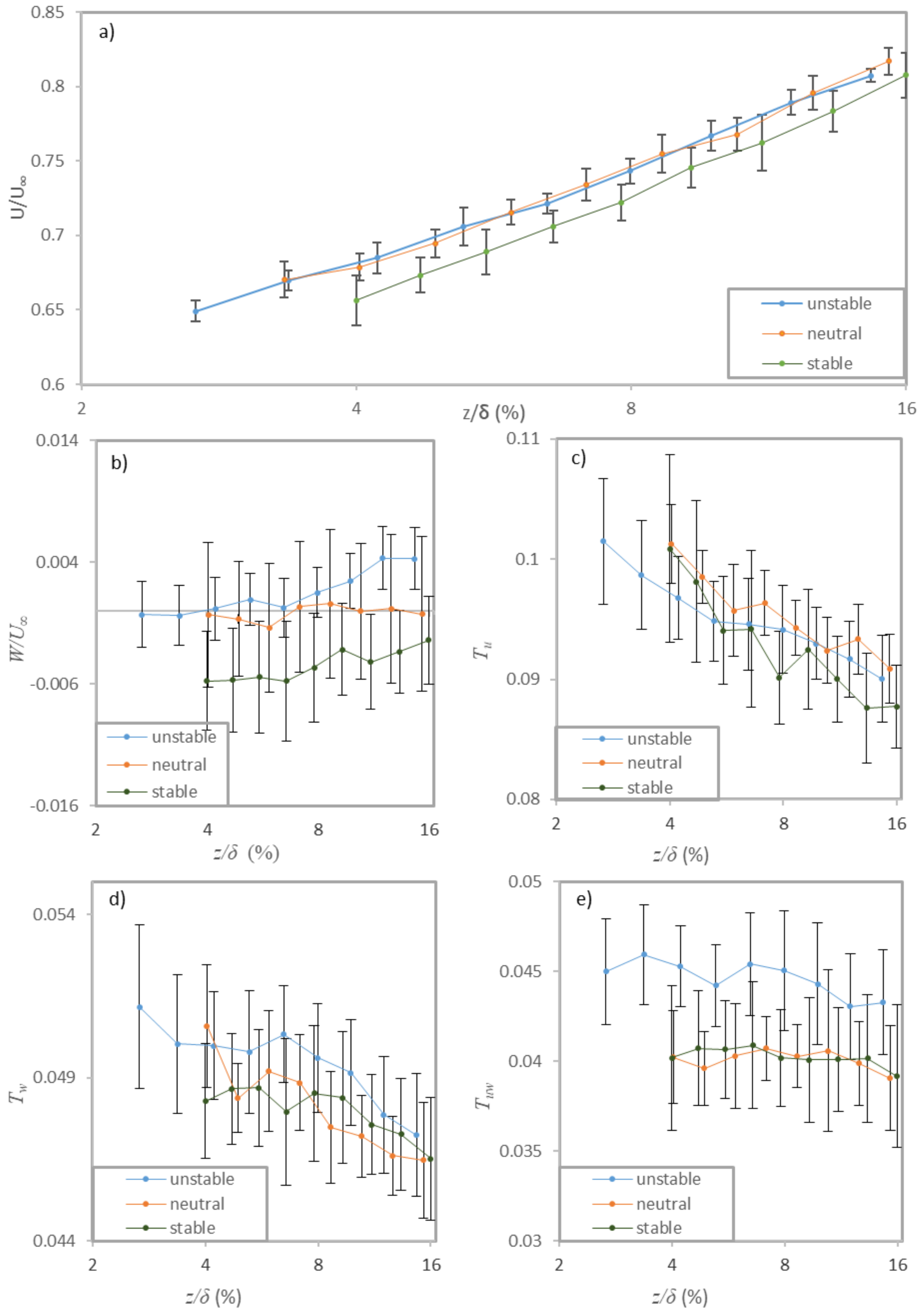

Fig. 2 Effect of atmospheric stability on vertical profiles of the flow velocity (a and b), turbulence intensity (c and d) and Reynolds stress (e). Error bars indicate the standard deviation for each bin.

In a similar way, we also derived the bin-averaged turbulence intensity (T_u, T_w) and dimensionless Reynolds stress (T_{uw}) profiles with their standard deviations for different stability conditions (c.f. Figs. 2c-2e). There is substantial variability in these profiles, which is similar to the vertical profiles of W/U_∞. The bin-averaged T_u and T_w profiles decrease in magnitude away from the bed surface, with T_u decreasing much faster than T_w. However, the Richardson number has no clear influence on these profiles. Finally, the individual T_{uw} profiles do not show any consistent trend with elevation, whereas the binned profiles shown in Fig. 2 (e) appear to display a minimal reduction, which is largest in unstable conditions, but still below 3%. Note that T_{uw} values are expected to be constant within the constant stress layer.

3.2 Parameterization of the Law of the Wall

Figure 3a reveals the apparent von Kármán parameter κ_a (Eqn 11) varies widely from 0.33 to 0.51 for Set 1 (blue dots), with a strong linear dependency on Ri (R^2 = 0.73 and p < 0.001, excluding two outliers denoted by black triangle symbols). The y-intercept indicates that the von Kármán constant for neutral conditions κ is 0.414. For Set 2 (red dots), which were solely run to examine the variability of κ under neutral conditions, the measurements obtained follow a right-skewed normal distribution with a mean ($\overline{\kappa}$) of 0.412 and a standard deviation of 0.0232, i.e., about 56 % of values lie between 0.39 and 0.42. In effect, excellent agreement is obtained between κ and $\overline{\kappa}$ derived for neutral conditions from both sets of experiments.

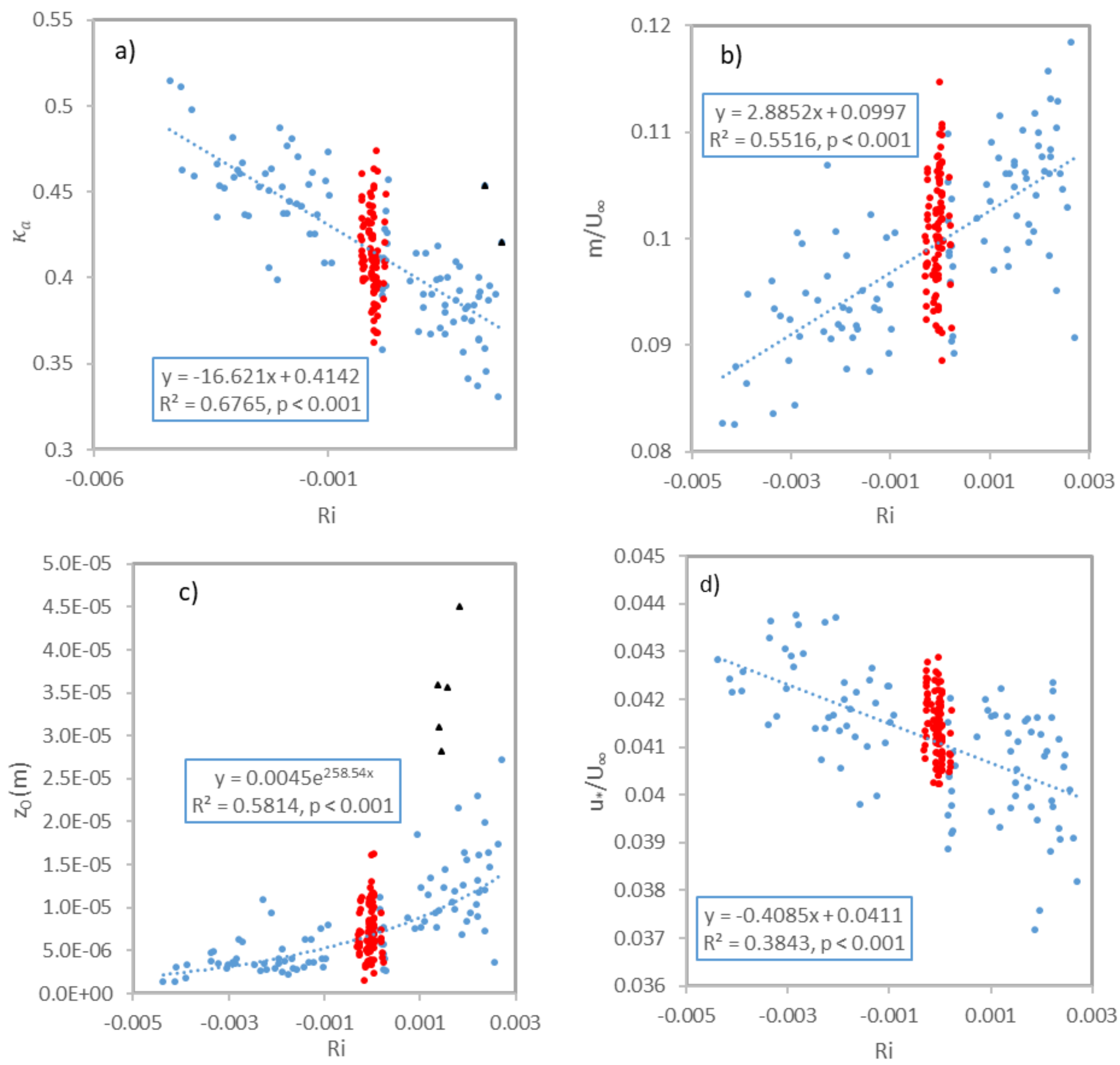

Fig. 3 Influence of atmospheric stability (*Ri)* on a) κ_a, b) m/U_∞, c) z_o and d) u_*/U_∞. Red point symbols pertain to Set 2 for neutral conditions only, as distinct from the remaining data collected from Set 1. Data shown as black triangles in c was not considered during regression analysis.

Further analysis of the streamwise velocity profiles from Set 1 shows that *m* (Fig. 3 c) and z_0 (Fig. 3d) derived from the Law of the Wall (Eqn 2) show very strong linear ($R^2 = 0.55$, $p < 0.001$) and exponential ($R^2 = 0.58$, $p < 0.001$) dependency on *Ri*, respectively. The overall variability in *m* and z_0 for stable experiments is larger than that for unstable experiments due to the difficulty in controlling surface roughness when misting the sand bed. In particular, one set of experiments is far away from the main point cloud (marked with black triangles), and thus have been removed from the exponential regression. The derived *m* and z_0 values from Set 2 fall in line with the projected linear regression based on data collected for Set 1. The normalized shear velocity u_*/u_∞ derived from Reynolds stress profiles (Exp 1) shows a linear decline with increasing thermal stability (Fig. 3e, $R^2 = 0.38$ and $p < 0.001$). However, the intercept is somewhat lower than the mean normalized friction velocity determined from Set 2.

4. Discussion

4.1 Stability controls on wind field

Our results show that time-averaged streamwise velocity (U) profiles are always log-linear regardless of their stability conditions, and with a linear increase in Ri, the apparent roughness lengths (z_0) rise exponentially, and the normalized slopes (m/U_∞) rise linearly. These results are consistent with previous wind tunnel (Ogawa et al. 1981, Sessa et al. 2020, Demarco et al. 2022) and field studies (Monin and Obukhov 1954, Frank and Kocurek 1994, Andreas et al. 2006, Salesky et al. 2013). In addition, a zero normalized vertical-velocity (W/U_∞) for neutral conditions is consistent with field and laboratory measurements (Ohya et al. 1996, Lee 2018) indicating an equilibrium between upward and downward directed movement of the air flow. In unstable conditions positive W/U_∞ values signal the occurrence of convectional air movement, and negative W/U_∞ values indicate the occurrence of sinking air. The convective flows tend to reduce the apparent surface roughness effect by reducing the compression force of air on the surface, while sinking air makes the apparent roughness effect more pronounced by enhancing air compression and inhibiting turbulent mixing (Zilitinkevich et al. 2008, Zhang et al. 2013). This study shows that both turbulence intensities (T_u and T_w) decrease with increasing elevation, while the dimensionless Reynolds stress (T_{uw}) remains almost constant within the constant stress layer, which is consistent with many other field and wind tunnel studies (Joffre 2001, Ohya 2001, Hara et al. 2009; Li and Mckenna Neumann 2012). The existence of a constant stress layer also validates our methodology to determine u_* (Nezu et al. 1997). Our results also confirm that stable stratified flows tend to have smaller T_w, T_{uw} and u_*/U_∞ (Hancock and Hayden, 2018) while thermally unstable flows tend to have larger values (Hansen 1993; Hancock et al., 2013). This difference suggests that the damping effect from stable stratification can compress eddies, while the convection effect from unstable stratification can enlarge them (Oke 1978). However, we find that our neutral profiles do not always lie inbetween the stable and unstable profiles, which is most obvious for T_u, T_w, and T_{uw} profiles. This result could be due to substantial variability in the turbulence measurements (c.f. Figs 2c-2e). A longer sampling period for each position could reduce such variability, however, the longer sampling duration would also result in more significant temperature changes, which may introduce more variability in the wind field measurement.

4.2 Stability controls on κ_a and $\emptyset_m$

Based on Prandtl's Mixing Length Theory (1925) and von Kármán's Similarity Theory (1931), κ_a is a scaling factor describing the eddy size. Atmospheric stability controls the eddy size, and thus a strong, negative, linear relationship between κ_a and *Ri* was observed in our study. Our derived κ value under neutral conditions (0.414) falls in the canonical value range, 0.37-0.42, as suggested by many fluid dynamic studies in the field and laboratory, such as Wieringa's (1980) re-evaluation of the Businger et al. (1971) data sets, Kondo and Sate (1982), Frenzen and Vogel (1995), Högström (1996), or Mckeon et al. (2004). Compared to the arctic sea ice SHEBA field study (Andreas et al. 2006), our κ_a range (0.33 ~ 0.51) largely overlaps theirs (0.24 ~ 0.58), indicating substantial variability under non-neutral conditions.

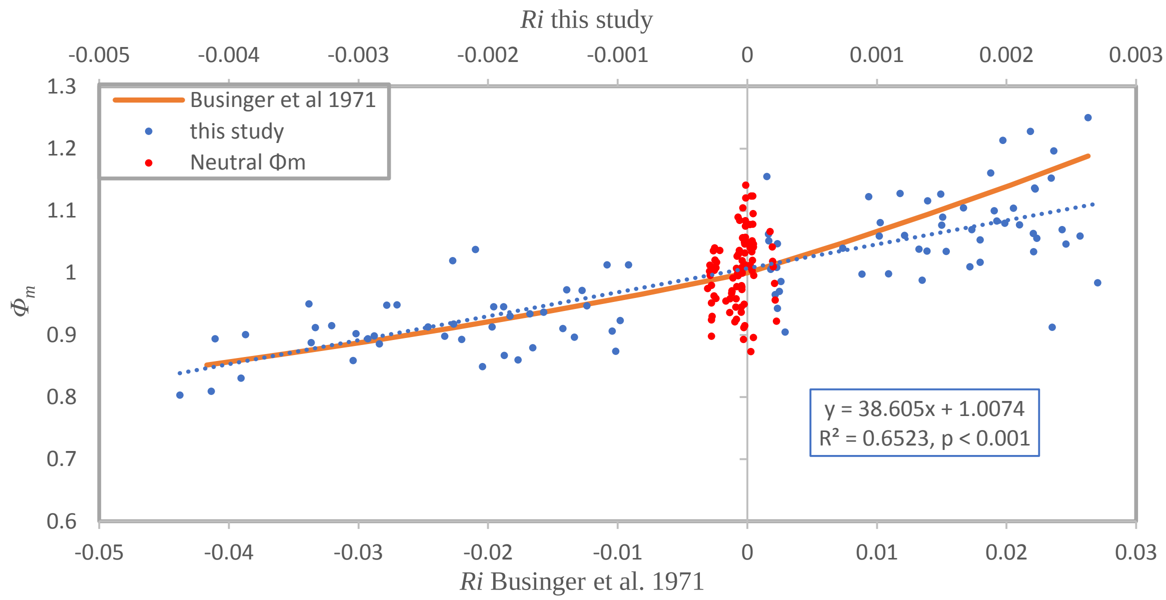

Fig. 4 Relationship between *Ri* and $\emptyset_m$

Most atmospheric studies report the dimensionless wind shear $\emptyset_m$, so we further transformed the reported κ_a to $\emptyset_m$ using Eq. 5 and $\kappa = 0.414$. Our $\emptyset_m$ has a relatively small range of 0.8 to 1.25, compared to the famous Kansas field study (Businger et al. 1971) with $\emptyset_m$ varying from below 0.8 to over 2. Regression analysis between $\emptyset_m$ and *Ri* reveals a strong positive, linear relationship between $\emptyset_m$ and *Ri* with $R^2 = 0.65$, $p < 0.001$. This relationship is similar to the Kansas study, provided their *Ri* is reduced by a factor of ten (c.f. Fig. 4). This adjustment arises from a difference in scale between the field and laboratory studies, since *Ri* is a function of scale dependent velocity and thermal gradients while $\emptyset_m$, defined as κ/κ_a, is likely to be scale independent.

4.3 Implications for aeolian research

In this study, we report on a dataset with detailed wind measurements obtained centimeters above the sand bed surface within the constant stress layer under varied stability conditions. Unlike previous studies adopting very low wind velocities of 0.7 – 1.9 m s^{-1} to maintain a large thermal difference between surface and the airflow (e.g., Ohya 2001, Hara et al. 2009, Hancock et al. 2013, Hancock and Hayden. 2018), we simulated a stratified boundary layer with the wind speed large enough to entrain fine sediment from a bed surface. These high wind velocities make our study not only important for understanding the stratification effect on wind profiles, turbulence intensity and momentum flux, but also relevant to the modelling of sediment entrainment and transport by wind.

Little is known about the effect of atmospheric stability on sediment entrainment. Our study shows that both the vertical velocity component and Reynolds stress are influenced by thermal stratification (c.f. Figs. 2b and 2e). Given sediment entrainment is normally driven by both lift and aerodynamic drag forces (Bagnold 1936; Shao and Lu, 2000) and vertical velocity and Reynolds stress can significantly affect these forces, the atmospheric stability may have a substantial effect on sediment entrainment. As shown in Fig. 2b, normalized vertical velocity W/U_{∞} in the constant stress layer had negative values for stable conditions and nearly 0 or positive values for unstable conditions. This vertical velocity direction change can significantly influence the lift force (Coulter and Martin 1996, Yang and Ishraq, 2021), i.e. increasing the lift in unstable air and decreasing the lift in stable air. In addition, the enhanced T_{uw} under unstable conditions exert stronger drag on the sand particles than under stable conditions. As both lift and drag forces have been raised in the unstable air and reduced in the stable air, decreasing atmospheric stability can enhance the probability of sand particle entrainment, and hence decrease the fluid threshold shear velocity u_{*t}. Since the fluid threshold shear velocity was not measured, further studies should focus on quantitatively evaluating the relationship between u_{*t} and Ri. The sediment transport rate Q is well recognized to be dependent on u_*^3 (Bagnold 1937, Zingg 1953), or $(u_* - u_{*t})u_*^2$ (Lettau and Lettau, 1978). Since the fluid stress is usually estimated from velocity profile measurements using a von Kármán constant κ of 0.4 (Eqn. 2), substantial errors may arise in wind erosion modelling when estimating u_* without considering the variability of κ_a under non-neutral atmospheric conditions. Based on our experiments, which addresses a narrow range of gradient Richardson numbers, κ_a can vary from 0.33 to 0.51, which can potentially result in an error of up to 23% in u_* estimation and up to 88% error in sediment transport rate Q prediction following Bagnold's and Zingg's models. For the Lettau and Lettau (1978) model, without knowing the concrete relationship between fluid threshold shear velocity u_{*t} and atmospheric stability, making definite conclusions is difficult. However, it is reasonable to make a qualitative evaluation. As atmospheric stability increases, u_* decreases while u_{*t} increases. This change leads to a decrease in $(u_* - u_{*t})u_*^2$ and thus a reduction in Q. Furthermore, these errors will also be translated to saltation induced dust emission models which also require the accurate estimations of u_* and u_{*t} (Ginoux et al. 2001, Shao 2001, LeGrand et al. 2019).

5. Conclusions

Our thermally controlled experiments simulated airflow under different stability conditions and characterized the time-averaged and instantaneous flow characteristics within the constant shear stress layer at millimetre scale resolution. The key results demonstrate that

1) Increasing atmospheric stability manifests as higher apparent aerodynamic roughness length (z_0) in vertical profiles of wind velocity.
2) Stable stratification supresses the turbulence intensity and dimensionless Reynolds stress, while unstable stratification has the opposite effect.
3) The apparent von Kármán parameter is inversely proportional to the integrated gradient Richardson number (Ri) with a value of 0.414 under neutral conditions.
4) Increasing atmospheric stability may lead to overestimation of shear velocity and transport rate, and underestimation of threshold shear velocity.

Acknowledgements: This research is financially supported by National Natural Science Foundation of China (Grant No. 41871005) and Xi'an Jiaotong-Liverpool University. The authors also greatly thank Dr. Patrick O'Brien for his valuable technical support.

6. References

Andreas, E. L., Claffey, K. J., Jordan, R. E., Fairall, C. W., Guest, P. S., Persson, P. O. G., & Grachev, A. A. (2006). Evaluations of the von Kármán constant in the atmospheric surface layer. Journal of Fluid Mechanics, 559, 117 - 149.

Bagnold, R. A. (1936). The movement of desert sand, Proc. R. Soc. London, Ser. A, 157(892), 594-620.

Bagnold, R. A. (1941). The Physics of Blown Sand and Desert Dunes (New York: Methuen).

Bauer, B. O., Sherman, D. J., & Wolcott, J. F. (1992). Sources of Uncertainty in Shear Stress and Roughness Length Estimates Derived from Velocity Profiles∗. The Professional Geographer, 44(4), 453–464.

Balsley, B. B., Svensson, G., & Tjernström, M. (2007). On the Scale-dependence of the Gradient Richardson Number in the Residual Layer. Boundary-Layer Meteorology, 127(1), 57–72.

Businger, J. A., Wyngaard, J. C., Izumi, Y., & Bradley, E. F. (1971). Flux-Profile Relationships in the Atmospheric Surface Layer. Journal of the Atmospheric Sciences, 28(2), 181–189.

Cantwell, B. J. (2019). A universal velocity profile for smooth wall pipe flow. Journal of Fluid Mechanics, 878, 834–874.

Cheng, Y., Li, Q., Li, D., & Gentine, P. (2021). Logarithmic profile of temperature in sheared and unstably stratified atmospheric boundary layers. Physical Review Fluids, 6(3).

Coulter, R. L., & Martin, T. J. (1996). Effects of stability on the profiles of vertical velocity and its variance in katabatic flow. Boundary-layer meteorology, 81(1), 23-33.

Li, D. (2018). Turbulent Prandtl Number in the atmospheric boundary layer - where are We now? Atmospheric Research.

Demarco G, Martins LGN, Bodmann BEJ, Puhales FS, Acevedo OC, Wittwer AR, Costa FD, Roberti DR, Loredo-Souza AM, Degrazia FC, Tirabassi T, Degrazia GA. (2022). Analysis of Thermal and Roughness Effects on the Turbulent Characteristics of Experimentally Simulated Boundary Layers in a Wind Tunnel. Int J Environ Res Public Health. 2022, 19, 5134.

Dupont, S., Rajot, J-L., Labiadh, M., Bergametti, G., Alfaro, S. C., Bouet, C., et al. (2018). Aerodynamic parameters over an eroding bare surface: Reconciliation of the law of the wall and eddy covariance determinations. Journal of Geophysical Research: Atmospheres, 123, 4490–4508.

Francey, R. J., & Garratt, J. R. (1981). Interpretation of Flux-Profile Observations at ITCE (1976). Journal of Applied Meteorology, 20(6), 603–618.

Frank, A., & Kocurek, G. (1994). Effects of atmospheric conditions on wind profiles and aeolian sand transport with an example from white sands national monument. Earth Surface Processes and Landforms, 19(8), 735–745.

Frenzen, P., & Vogel, C. A. (1995). On the magnitude and apparent range of variation of the von Karman constant in the atmospheric surface layer. Boundary-Layer Meteorology, 72(4), 371–392.

Friedrich, K., Lundquist, J. K., Aitken, M., Kalina, E. A., & Marshall, R. F. (2012). Stability and turbulence in the atmospheric boundary layer: A comparison of remote sensing and tower observations. Geophysical Research Letters, 39(3).

Garratt, J. (1994). Review: the atmospheric boundary layer. Earth-Science Reviews, 37(1-2), 89–134. doi:10.1016/0012-8252(94)90026-4

Ginoux, P., Chin, M., Tegen, I., Prospero, J. M., Holben, B., Dubovik, O., & Lin, S.-J. (2001). Sources and distributions of dust aerosols simulated with the GOCART model. Journal of Geophysical Research: Atmospheres, 106(D17), 20255–20273.

Hara, T., Ohya, Y., Uchida, T., & Ohba, R. (2009). Wind-Tunnel and Numerical Simulations of the Coastal Thermal Internal Boundary Layer. Boundary-Layer Meteorology, 130(3), 365–381.

Hancock, P. E., & Hayden, P. (2018). Wind-Tunnel Simulation of Weakly and Moderately Stable Atmospheric Boundary Layers. Boundary-Layer Meteorology, 168(1), 29–57.

Hancock, P. E., Zhang, S., & Hayden, P. (2013). A Wind-Tunnel Artificially-Thickened Simulated Weakly Unstable Atmospheric Boundary Layer. Boundary-Layer Meteorology, 149(3), 355–380.

Hansen, F. V. (1993). Surface roughness lengths. Army Research Lab White Sands Missile Range Nm.

Högström, U. (1996). Review of some basic characteristics of the atmospheric surface layer. Boundary-Layer Meteorology, 78(3-4), 215–246.

Högström, U., Sahlée, E., Drennan, W.M., Kahma, K.K., Smedman, A.S., Johansson, C., Pettersson, H., Rutgersson, A., Tuomi, L., Zhang, F.M., & Johansson, M.M. (2008). Momentum fluxes and wind gradients in the marine boundary layer: a multi platform study. Boreal Environment Research, 13, 475-502.

Joffre, S. M., Kangas, M., Heikinheimo, M., & Kitaigorodskii, S. A. (2001). Variability Of The Stable And Unstable Atmospheric Boundary-Layer Height And Its Scales Over A Boreal Forest. Boundary-Layer Meteorology, 99(3), 429–450.

Kawamura, R., 1951. Study of sand movement by wind, The reports of the Institute of Science and Technology: vol 5. University of Tokyo, Tokyo, Japan, 95–112.

Kim, D.-Y., Kim, Y.-H., & Kim, B.-S. (2020). Changes in wind turbine power characteristics and annual energy production due to atmospheric stability, turbulence intensity, and wind shear. Energy, 119051.

Kok, J. F., Parteli, E. J. R., Michaels, T. I., & Karam, D. B. (2012). The physics of wind-blown sand and dust. Reports on Progress in Physics, 75(10), 106901.

Kondo, J., & Sate, T. (1982). The determination of the von Kármán constant. Journal of the Meteorological Society of Japan. Ser. II, 60(1), 461-471.

Lee, Xuhui. Fundamentals of boundary-layer meteorology. Vol. 256. Gewerbestrasse: Springer International Publishing.

LeGrand, S. L., Polashenski, C., Letcher, T. W., Creighton, G. A., Peckham, S. E., & Cetola, J. D. (2019). The AFWA dust emission scheme for the GOCART aerosol model in WRF-Chem v3. 8.1, Geosci. Model Dev., 12, 131–166.

Lettau, K., Lettau, H., (1978). Experimental and micrometeorological field studies of dune migration. In: Lettau, K., Lettau, H. (Eds.), Exploring the World’s Driest Climate. Center for Climatic Research, University of Wisconsin-Madison, 110–147, IES Report 101.

Li, Bailiang (2010). Evaluating the von Kármán Constant in Sediment-laden Air Flow. Doctoral dissertation, Texas A&M University.

Li, B., Ellis, J. T., & Sherman, D. J. (2014). Estimating the impact threshold for wind-blown sand. Journal of Coastal Research, 70, 627–632.

Li, B., Sherman, D. J., Farrell, E. J., & Ellis, J. T. (2010). Variability of the apparent von Kármán parameter during aeolian saltation. Geophysical Research Letters, 37(15).

Li, B., & McKenna Neuman, C. (2012). Boundary-layer turbulence characteristics during aeolian saltation. Geophysical Research Letters, 39(11).

Li, D. (2018). Turbulent Prandtl Number in the atmospheric boundary layer - where are We now? Atmospheric Research.

Mahrt, L. (2007). The influence of nonstationarity on the turbulent flux–gradient relationship for stable stratification. Boundary-Layer Meteorology, 125(2), 245–264.

Marucci, D., Carpentieri, M., & Hayden, P. (2018). On the simulation of thick non-neutral boundary layers for urban studies in a wind tunnel. International Journal of Heat and Fluid Flow, 72, 37–51.

Marusic, I., McKeon, B. J., Monkewitz, P. A., Nagib, H. M., Smits, A. J., & Sreenivasan, K. R. (2010). Wall-bounded turbulent flows at high Reynolds numbers: Recent advances and key issues. Physics of Fluids, 22(6), 065103.

Mckenna Neuman, C. (2003). Effects of temperature and humidity upon the entrainment of sedimentary particles by wind. Boundary-Layer Meteorology, 108(1), 61-89

McKenna Neuman, C., Li, B., & Nash, D. (2012). Micro‐ topographic analysis of shell pavements formed by aeolian transport in a wind tunnel simulation. Journal of Geophysical Research: Earth Surface, 117(F4).

Mckeon, B. J., Li, J. D., Jiang, W., Morrison, J. F., & Smits, A. J. (2004). Further observations on the mean velocity distribution in fully developed pipe flow. Journal of Fluid Mechanics, 501, 135-147

Monin, A. S., & Obukhov, A. M. (1954). Basic laws of turbulent mixing in the surface layer of the atmosphere. Contrib. Geophys. Inst. Acad. Sci. USSR, 151(163).

Monty J. P. (2005). Developments in smooth wall turbulent duct flows, Ph.D. thesis, University of Melbourne.

Morrison, J. F., McKeon, B. J., Jiang, W., & Smits, A. J. (2004). Scaling of the streamwise velocity component in turbulent pipe flow. Journal of Fluid Mechanics, 508, 99–131.

Mortensen, Niels & Larsen, Søren & Troen, I. & Mikkelsen, Torben. (1987). Two years worth of turbulence data recorded by a sonic-anemometer-based data acquisition system. Conference: Sixth Symposium on Meteorology and Instrumentation. At: New Orleans, Louisiana, American Meteorological Society, Boston, Mass., US

Nagib, H. M., Chauhan, K. A., & Monkewitz, P. A. (2007). Approach to an asymptotic state for zero pressure gradient turbulent boundary layers. Philosophical transactions. Series A, Mathematical, physical, and engineering sciences, 365(1852), 755–770.

Neuman, C. M. (2004). Effects of temperature and humidity upon the transport of sedimentary particles by wind. Sedimentology, 51(1), 1–17.

Nezu, I., Kadota, A., & Nakagawa, H. (1997). Turbulent Structure in Unsteady Depth-Varying Open-Channel Flows. Journal of Hydraulic Engineering, 123(9), 752–763.

Nickels, T., Marusic, I., Hafez, S., Hutchins, N., & Chong, M. . (2007). Some predictions of the attached eddy model for a high Reynolds number boundary layer. Philosophical Transactions of the Royal Society A: Mathematical, Physical and Engineering Sciences, 365(1852), 807–822.

Nickling, W. G., & McKenna Neuman, C. (1997). Wind tunnel evaluation of a wedge-shaped aeolian sediment trap. Geomorphology, 18(3-4), 333–345.

Prandtl, L. (1925). 7. Bericht über Untersuchungen zur ausgebildeten Turbulenz. ZAMM – Journal of Applied Mathematics and Mechanics / Zeitschrift Für Angewandte Mathematik Und Mechanik, 5(2), 136–139.

Rana, S., Anderson, W., Day, M., 2020. Turbulence‐ based model for subthreshold aeolian saltation. Geophysical Research Letters, 47(15), e2020GL088050.

Salesky, S. T., Katul, G. G., & Chamecki, M. (2013). Buoyancy effects on the integral lengthscales and mean velocity profile in atmospheric surface layer flows. Physics of Fluids, 25(10).

Shao, Y. (2001). A model for mineral dust emission. Journal of Geophysical Research: Atmospheres, 106(D17), 20239–20254.

Shao, Y., & Lu, H. (2000). A simple expression for wind erosion threshold friction velocity. Journal of Geophysical Research: Atmospheres, 105(D17), 22437–22443.

Sessa, V., Xie, Z.-T., & Herring, S. (2020). Thermal Stratification Effects on Turbulence and Dispersion in Internal and External Boundary Layers. Boundary-Layer Meteorology.

Sherman, D. J., & Li, B. (2012). Predicting aeolian sand transport rates: A reevaluation of models. Aeolian Research, 3(4), 371–378.

Sørensen, M., (2004). On the rate of aeolian sand transport. Geomorphology 59, 53– 62.

Ogawa, Y., Diosey, P. G., Uehara, K., & Ueda, H. (1981). A wind tunnel for studying the effects of thermal stratification in the atmosphere. Atmospheric Environment (1967), 15(5), 807–821.

Ohya, Y., Tatsuno, M., Nakamura, Y., & Ueda, H. (1996). A thermally stratified wind tunnel for environmental flow studies. Atmospheric environment, 30(16).

Ohya, Y. (2001). Wind-Tunnel Study Of Atmospheric Stable Boundary Layers Over A Rough Surface. Boundary-Layer Meteorology, 98(1), 57–82.

Ohya, Y., & Uchida, T. (2004). Laboratory and Numerical Studies of the Convective Boundary Layer Capped by a Strong Inversion. Boundary-Layer Meteorology, 112(2), 223–240.

Oke, T. 1978. Boundary Layer Climates. London: Methuen & Co Ltd.Owen, P. (1964). Saltation of uniform grains in air. Journal of Fluid Mechanics, 20(2), 225-242.

Österlund, J. M., Johansson, A. V., Nagib, H. M., & Hites, M. H. (2000). A note on the overlap region in turbulent boundary layers. Physics of Fluids, 12(1), 1–4.

Uchida, T., & Ohya, Y. (1999). Numerical simulation of atmospheric flow over complex terrain. Journal of Wind Engineering and Industrial Aerodynamics, 81(1-3), 283–293.

Von Kármán, T. (1931). Mechanical similitude and turbulence (No. 611). National Advisory Committee for Aeronautics.

Wieringa, J. (1980). A revaluation of the Kansas mast influence on measurements of stress and cup anemometer overspeeding. Boundary-Layer Meteorology, 18(4), 411–430.

Wiggs, G. f. S., Atherton, R. J., & Baird, A. J. (2004). Thresholds of aeolian sand transport: establishing suitable values. Sedimentology, 51(1), 95–108.

Wright, S., & Parker, G. (2004). Density Stratification Effects in Sand-Bed Rivers. Journal of Hydraulic Engineering, 130(8), 783–795.

Wyngaard, J. C., Businger, J. A., Kaimal, J. C., & Larsen, S. E. (1982). Comments on a revaluation of the Kansas mast influence on measurements of stress and cup anemometer overspeeding? Boundary-Layer Meteorology, 22(2), 245–250.

Yang, S. Q., & Ishraq, A. F. (2021). Formulae of Sediment Transport in Steady Flows (Part 1). In Sediment Transport-Recent Advances. IntechOpen.

Zhang, Q., Wang, S., Barlage, M., Tian, W., & Huang, R. (2011). The characteristics of the sensible heat and momentum transfer coefficients over the Gobi in Northwest China. International Journal of Climatology, 31(4), 621–629.

Zhang, Q., Yao, T., Yue, P., Zhangf, L., & Zeng, J. (2013). The influences of thermodynamic characteristics on aerodynamic roughness length over land surface. Acta Meteorologica Sinica, 27(2), 249–262.

Zheng, X., Jin, T., Wang, P., 2020. The influence of surface stress fluctuation on saltation sand transport around threshold. Journal of Geophysical Research: Earth Surface, 125(5), e2019JF005246.

Zanoun, E.-S., Durst, F., & Nagib, H. (2003). Evaluating the law of the wall in two-dimensional fully developed turbulent channel flows. Physics of Fluids, 15(10), 3079.

Zilitinkevich, S. S., Mammarella, I., Baklanov, A. A., & Joffre, S. M. (2008). The Effect of Stratification on the Aerodynamic Roughness Length and Displacement Height. Boundary-Layer Meteorology, 129(2), 179–190.

Zingg, A.W., (1953). Wind tunnel studies of the movement of sedimentary material. In: Proceedings, 5th Hydraulics Conference, Studies in Engineering 34, 111- 135.